Inorganic Chemistry

Article

pubs.acs.org/IC

Density Functional Theory Studies on the Oxidation of 5′-dGMP and 5′-dAMP by a Platinum(IV) Complex

Alireza Ariafard,*[,†] Elham S. Tabatabaie,[†] Simin Aghmasheh,[†] Sahar Najaflo,[†] and Brian F. Yates*[,‡]

[†]Department of Chemistry, Faculty of Science, Central Tehran Branch, Islamic Azad University, Shahrak Gharb, Tehran, Iran

[‡]School of Chemistry, University of Tasmania, Private Bag 75, Hobart TAS 7001, Australia

Supporting Information

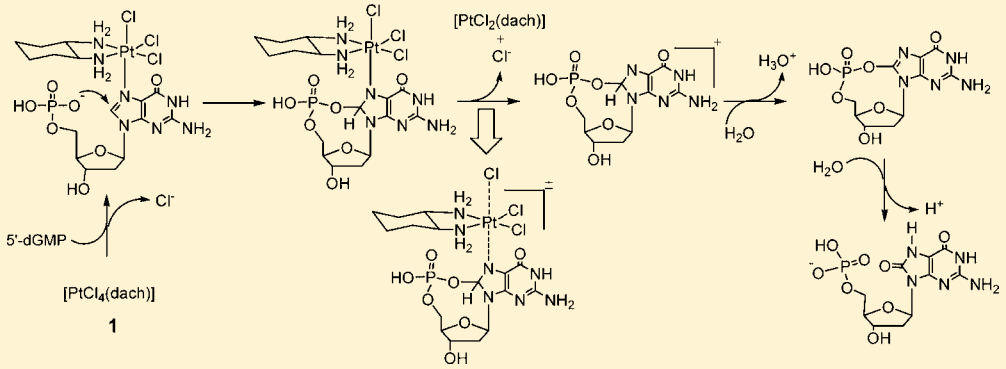

ABSTRACT: Density functional theory has been used to investigate the oxidation of a guanine nucleotide by platinum(IV), a process that can be important in the degradation of DNA. For the first time, we have provided a comprehensive mechanism for all of the steps in this process. A number of intermediates are predicted to occur but with short lifetimes that would make them difficult to observe experimentally. A key step in the mechanism is electron transfer from guanine to platinum(IV), and we show that this is driven by the loss of a chloride ligand from the platinum complex after nucleophilic attack of 5′-phosphate to C8 of guanine. We have investigated several different initial platinum(IV) guanine adducts and shown that the adduct formed from replacement of an axial chlorine ligand in the platinum(IV) complex undergoes oxidation more easily. We have studied adenine versus guanine adducts, and our results show that oxidation of the former is more difficult because of disruption of the aromatic π system that occurs during the process. Finally, our results show that the acidic hydrolysis step to form the final oxidized product occurs readily via an initial protonation of N7 of the guanine.

INTRODUCTION

The oxidation of nucleobases,[1] which subsequently results in an alteration in the DNA structure, can lead to processes such as aging, mutagenesis, carcinogenesis, and death.[2] It is well established that many metals are capable of promoting/catalyzing the oxidative transformations of nucleobases.[3] In this regard, Choi and co-workers investigated the oxidative behavior of some platinum(IV) complexes toward DNA and showed that these complexes are able to oxidize guanine (G) nucleotides such as 5′-dGMP, 3′-dGMP, and 5′-[GTTTT]-3′ through a consecutive two-step inner-sphere mechanism.[4] They found that a crucial requirement in order for the redox reaction to occur is that guanine must have a hydroxyl or a phosphate nucleophile at its 5′ position.[4c,d] Scheme 1 shows the proposed mechanism for the oxidation of 5′-dGMP by [$Pt^{IV}Cl_4$(dach)] (**1**; dach = diaminocyclohexane).[4c] Accordingly, the reaction proceeds via coordination of the N7 of guanine to Pt^{IV}, forming **2_G**, followed by the transfer of two electrons from guanine to Pt^{IV} as a result of nucleophilic attack of 5′-phosphate to C8 of guanine to give a platinum(II) complex and a cyclic phosphodiester intermediate (Scheme 1). However, this phosphodiester intermediate is not stable at all and is hydrolyzed to 8-oxo-5′-dGMP (Scheme 1). The rate of the hydrolysis process depends on the pH and increases with decreasing pH.

Although parts of the mechanism of this reaction have been verified experimentally in detail, still a number of interesting questions remain to be answered. These questions are as follows: (1) What intermediate(s) are likely formed during the course of the guanine oxidation? (2) Because there is no evidence for the formation of **3_G** experimentally, we want to know whether this species is an intermediate or not. If so, what is the reason that it cannot be experimentally identified? (3) Can intermediate **3_G** (if it exists) be deprotonated in order to form the cyclic phosphodiester intermediate? If not, which intermediate is responsible for the deprotonation process? (4) What is the mechanism of electron transfer from guanine to Pt^{IV}? (5) Two different chloro ligands, axial and equatorial, are available to be substituted by guanine to give intermediates

Received: January 6, 2012
Published: July 18, 2012

   dx.doi.org/10.1021/ic300038m | *Inorg. Chem.* 2012, 51, 8002−8013

Scheme 1

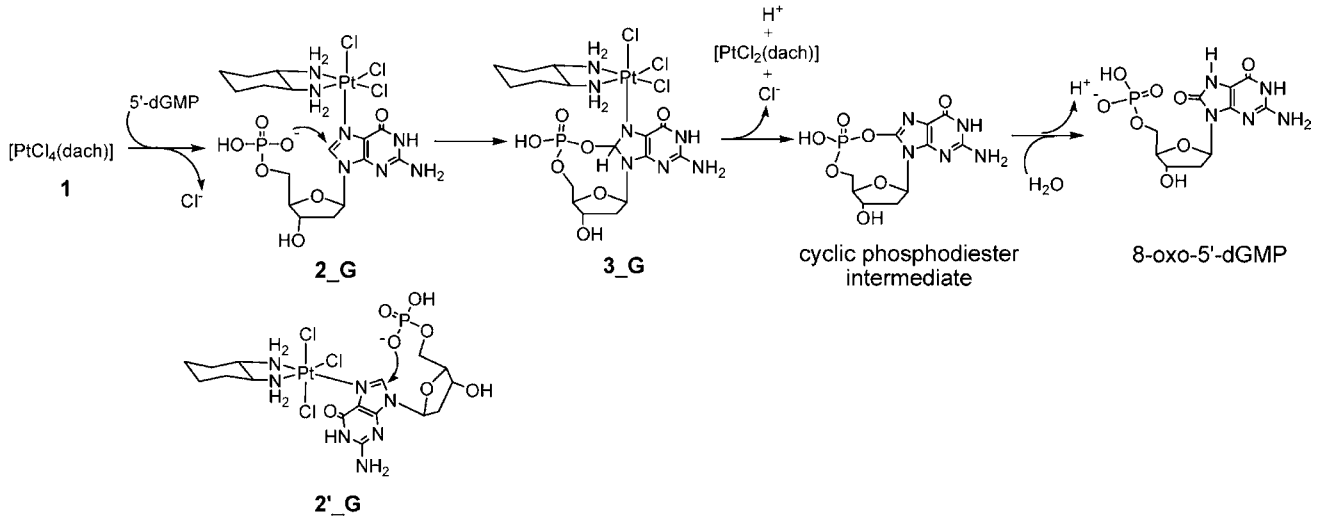

2_G and **2′_G** (Scheme 1), respectively. Which one of them can undergo the guanine oxidation faster? (6) To date, only guanine nucleotides have been reported to be reactive toward oxidation. Taking this into account, is there any possibility for adenine nucleotides to be oxidized by platinum(IV) complexes? If not, what is the reason for this? (7) What is the mechanism for conversion of the cyclic phosphodiester intermediate to 8-oxo-5′-dGMP, and why is this reaction accelerated in acidic media? This work is aimed at addressing these important questions with the aid of density functional theory (DFT) calculations by providing a mechanistic picture of this process. Theoretical investigation of the oxidation of 3′-dGMP by Pt^{IV} is a subject of ongoing study and will be reported elsewhere.

COMPUTATIONAL METHODS

Gaussian 09[5] was used to fully optimize all of the structures reported in this paper in water using the CPCM solvation model[6] at the B3LYP level of DFT.[7] The effective-core potential of Hay and Wadt with a double-ξ valence basis set (LANL2DZ)[8] was chosen to describe Pt. The 6-31G(d) basis set was used for other atoms.[9] A polarization function of ξ_f = 0.993 was also added to Pt.[10] This basis set combination will be referred to as BS1. Frequency calculations were carried out at the same level of theory as those for the structural optimization. Transition states were located using the Berny algorithm. Intrinsic reaction coordinate (IRC)[11] calculations were used to confirm the connectivity between transition structures and minima. To further refine the energies obtained from the B3LYP/BS1 calculations, we carried out single-point energy calculations for all of the structures with a larger basis set (BS2) in water using the CPCM solvation model at the B3LYP and M06[12] levels. BS2 utilizes the quadruple-ζ valence def2-QZVP[13] basis set on Pt and the 6-311+G(2d,p) basis set on other atoms. We have used the potential and Gibbs free energies obtained from the B3LYP/BS2//B3LYP/BS1 calculations in water throughout the paper unless otherwise stated. The results related to the M06/BS2//B3LYP/BS1 calculations are included in the Supporting Information. The partial atomic charges and atomic orbital populations were calculated on the basis of natural bond orbital (NBO) analyses.[14]

RESULTS AND DISCUSSION

1. Oxidation of 5′-dGMP by $[Pt^{IV}Cl_4(dach)]$ via Substitution of an Axial Cl Ligand by 5′-dGMP. An inner-sphere mechanism that begins with the binding of Pt^{IV} to the N7 of the guanine moiety is considered for this reaction. The calculated energy profile for the reaction of 5′-dGMP with $[Pt^{IV}Cl_4(dach)]$, which gives the cyclic phosphodiester intermediate, is shown in Figure 1. (1*R*,2*R*)-1,2-Diaminocyclohexane was chosen to model the dach ligand in this study.

*1.1. Ligand Substitution and Nucleophilic Attack at C8 (**1** → **2_G** → **3_G**).* As can be seen from Figure 1a, the product of the axial Cl substitution is the Pt^{IV}−G adduct **2_G**. Our calculations showed that the N−H protons of the dach ligand interact simultaneously with the C6O carbonyl and the 5′-phosphate, as evidenced by elongation of the N−H bonds (Figure 2). Such hydrogen-bonding interactions can contribute to the stability of the Pt^{IV}−G adduct **2_G**.[15] The free energy change for the reaction of **1** + 5′-dGMP → **2_G** + Cl^- is calculated to be 4.8/−20.1 kJ mol^{-1}, where the values calculated at the B3LYP and M06 levels are listed before and after the slash, respectively. This result indicates that the substitution reaction is almost thermoneutral. The chloride substitution in the d^6 octahedral platinum complex usually occurs through a dissociative mechanism (Figure 1). The barrier for this dissociation reaction is predicted to be quite high: 140 and 182 kJ mol^{-1} at the B3LYP and M06 levels, respectively. The potential energy for complete dissociation of Cl^- is usually considered as the reaction barrier, with the assumption that the entropic effect of Cl^- loss in the transition structure is negligible.[16] However, Choi and co-workers showed that the substitution reaction does not occur through the dissociative pathway and is catalyzed by platinum(II) complexes.[17] This interesting observation deserves to be investigated theoretically in more detail, but this falls outside of the scope of the present study.

The coordination of N7 of 5′-dGMP to Pt^{IV} leads to a polarization of the C8−N7 π bond toward N7, increasing the positive charge on C8 from 0.209 in 5′-dGMP to 0.326 in **2_G**, consequently enhancing the electrophilicity of C8. The nucleophilic attack of 5′-phosphate to C8 of the guanine moiety through transition structure **1TS_G** leads to the formation of intermediate **3_G** (Figure 1).[18] In this process, the O of 5′-phosphate not involved in the hydrogen bonding (O^b) attacks the C8 atom, while O^a preserves its hydrogen bond with NH_2 of dach (Figure 2).[19] **1TS_G** has one imaginary frequency (287.07i) corresponding to the O^b−C8 stretching.

*1.2. Can **3_G** Be Deprotonated Directly by Water?* It is expected that deprotonation of **3_G** by water yields the cyclic phosphodiester intermediate. To simulate whether **3_G** can be

dx.doi.org/10.1021/ic300038m | Inorg. Chem. 2012, 51, 8002−8013

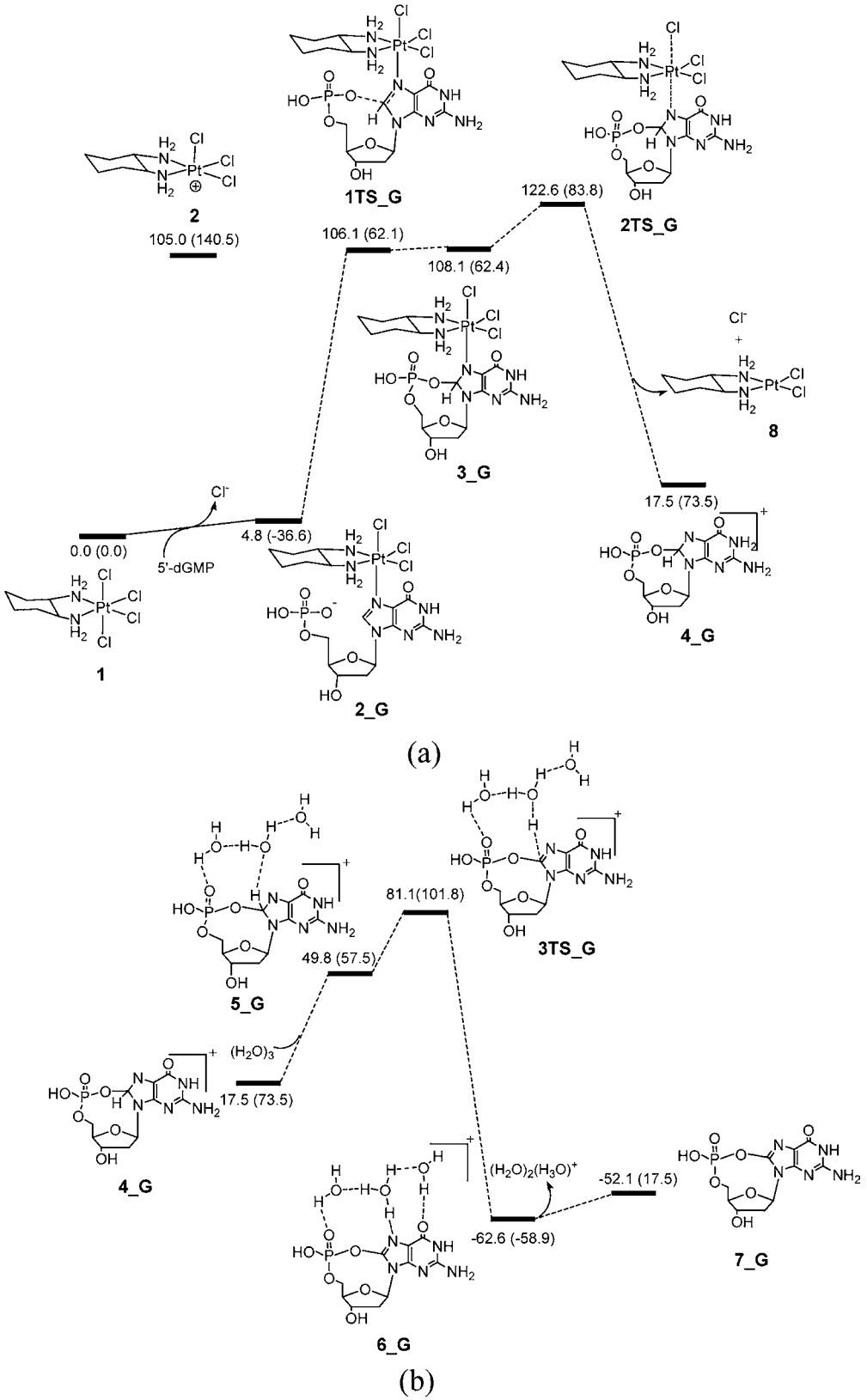

Figure 1. Energy profile calculated for the oxidation of 5′-dGMP by [Pt^{IV}Cl4(dach)] leading to (a) the formation of the cationic intermediate **4_G** and subsequently to (b) **7_G** through deprotonation of **4_G** by water. The relative free energies and electronic energies (in parentheses) obtained from the B3LYP/BS2//B3LYP/BS1 calculations are given in kJ mol^{-1}.

deprotonated by water, a three-water cluster[20] was considered. We were able to find transition structure **TS_G** for deprotonation of **3_G**, but our calculations indicated that this process occurs with concomitant dissociation of both the axial Cl and cyclic phosphodiester ligands from the platinum(IV) complex. The Pt−Cl_{ax} and Pt−N7 distances in **TS_G** are

dx.doi.org/10.1021/ic300038m | Inorg. Chem. 2012, 51, 8002−8013

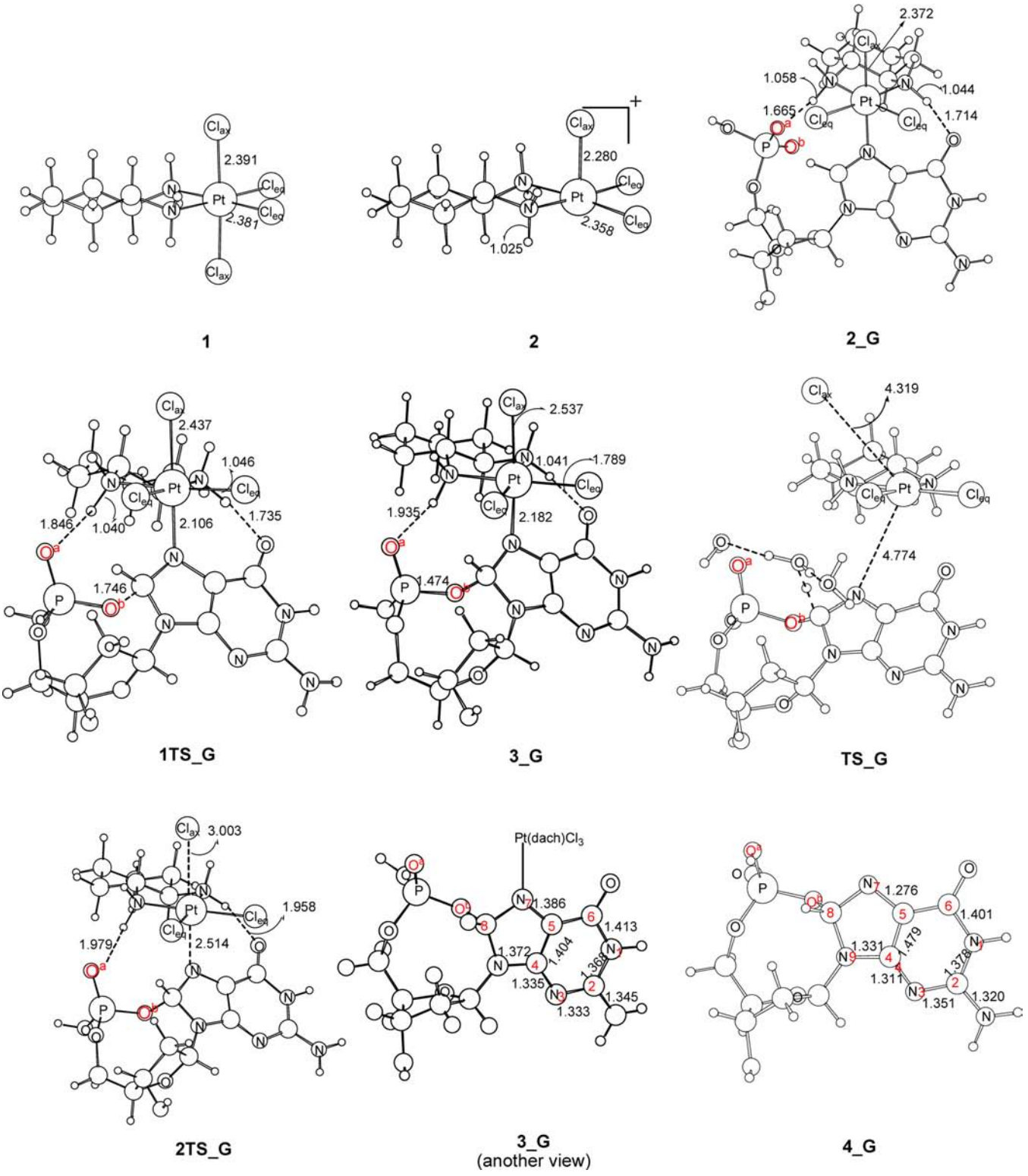

Figure 2. Optimized structures with selected structural parameters (bond lengths in Å) for **TS_G** and some of the species involved in the energy profiles shown in Figure 1.

calculated to be 4.319 and 4.774 Å, respectively (Figure 2), which are large enough to ensure that there is no covalent interaction between Pt and Cl_{ax} and between Pt and N7.

In order to confirm which structures the transition structure **TS_G** is connected to, we performed IRC calculations. The IRC calculations indicate that **TS_G** is connected to Cl^- + $Pt^{II}Cl_2$(dach) + **5_G** as the reactants and not to the hydrated **3_G**. We also found that H8-deprotonated **3_G** is not a minimum, and all attempts to locate this intermediate led to $Pt^{II}Cl_2$(dach), Cl^-, and **4_G**. These results suggest that, in order for the deprotonation process to occur, **3_G** should be initially decomposed into Cl^-, $Pt^{II}Cl_2$(dach), and **4_G**. In other words, Pt^{IV} should be reduced to Pt^{II} at first, forming the

dx.doi.org/10.1021/ic300038m | Inorg. Chem. 2012, 51, 8002−8013

Scheme 2

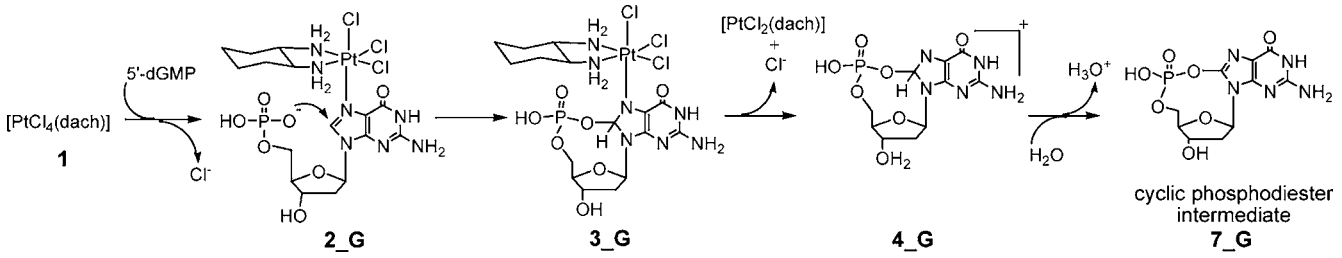

Table 1. NBO Partial Charges Concentrated on the Subunits $Pt(Cl_{eq})_2(dach)$, Cl_{ax}, and Guanine Moiety and Electron Population of the Pt $5d_{z^2}$, Cl_{ax} $3p_z$, Cl_{ax} 3s, and N7 $2p_z$ Orbitals along the Redox Reaction

	partial NBO charge on						
species	$Pt(Cl_{eq})_2(dach)$	Cl_{ax}	guanine moiety	$5d_{z^2}$ (Pt)	$3p_z$ (Cl_{ax})	3s (Cl_{ax})	$2p_z$ (N7)
2_G	0.686	−0.262	−0.424	1.189	1.439	1.873	1.441
1TS_G	0.638	−0.337	−0.302	1.227	1.507	1.887	1.351
3_G	0.549	−0.409	−0.140	1.308	1.569	1.907	1.296
2TS_G	0.336	−0.567	0.231	1.516	1.710	1.963	1.244

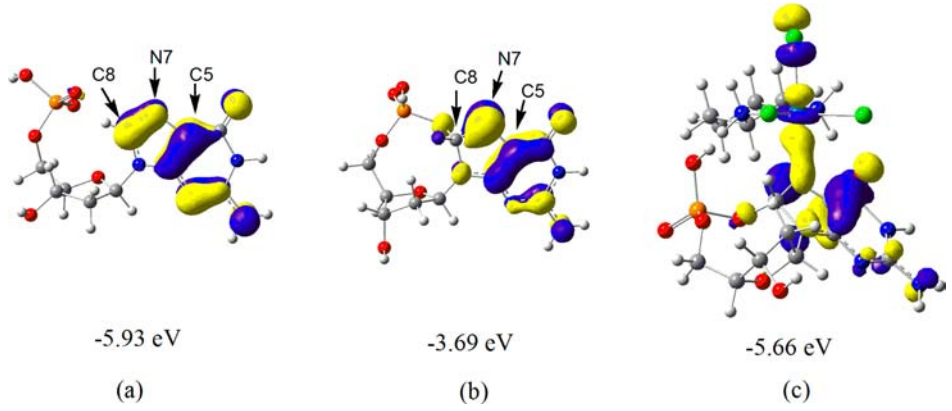

Figure 3. Spatial plots and energies for the HOMO of (a) the distorted 5′-dGMP moiety in **2_G**, (b) the distorted anionic phosphodiester moiety in **3_G**, and (c) **3_G**.

protonated intermediate **4_G**, and then **4_G** is deprotonated by water to produce **7_G** (Figure 1).[21]

1.3. Redox Step and Deprotonation of 4_G (3_G → 4_G → 7_G). Our calculations show that the reduction of Pt^{IV} is a very easy process that takes place via transition structure **2TS_G** with a free energy barrier as low as 14.5 kJ mol^{-1} (the energy difference between **3_G** and **2TS_G**). The M06/BS2//B3LYP/BS1 calculations also predict a small barrier (15.8 kJ mol^{-1}; Figure S2 in the Supporting Information) for the conversion of **3_G** to **4_G** + Cl^- + $Pt^{II}Cl_2(dach)$. Both the B3LYP and M06 calculations show that **2TS_G** is slightly higher in energy than **3_G** (Figures 1 and S2 in the Supporting Information). These results support the fact that **3_G** is very active toward the redox reaction. **2TS_G** has one imaginary frequency (84.76i), corresponding to the stretching of Pt−Cl_{ax} and Pt−N7 bonds moving in opposite directions. Starting from **2_G**, the overall Gibbs activation barriers for the oxidation of 5′-dGMP at the B3LYP and M06 levels and 298 K are calculated as 117.8 and 91.4 kJ mol^{-1}, respectively (Figures 1 and S1 in the Supporting Information). These results indicate that the M06 result somehow matches better with the experimental value ($\Delta G^{\ddagger}$ = 99.4 kJ mol^{-1}).[4e] What is very intriguing is that the reduction of Pt^{IV} (oxidation of guanine) takes place through elongation of the Pt−Cl_{ax} bond; a complete dissociation of the axial Cl^- ligand from **3_G** causes two electrons from the guanine moiety of the phosphodiester to be transferred to Pt^{IV}, and consequently the Pd−N7 bond is cleaved. Indeed, we found that weakening of the Pd−Cl_{ax} bond results in weakening of the Pt−N7 bond as well; on going from **3_G** to **2TS_G**, both the Pt−Cl_{ax} and Pt−N7 bonds are elongated by 0.466 and 0.332 Å, respectively (Figure 2). This result is opposite to what we expect based on the trans influence in transition-metal chemistry; for example, the loss of the Cl^- ligand from **1** strengthens the Pt−Cl_{ax} bond in **2**, as evidenced by a shorter Pd−Cl_{ax} bond; the Pt−Cl_{ax} bond distance is 2.391 and 2.281 Å in **1** and **2**, respectively (Figure 2). This is not the case for the Cl^- dissociation from **3_G**; when the Pt−Cl_{ax} bond is broken, the cationic species **4_G** is released and Pt^{IV} is reduced to Pt^{II}. The reason for this discrepancy, which is related to the superior ability of the coordinated cyclic phosphodiester for reducing Pt^{IV}, will be discussed in the next section.

Once the transition structure **2TS_G** is overcome, the guanine moiety is oxidized and **4_G** is formed. The overall reaction energy for the formation of **4_G** is calculated to be 17.5 kJ mol^{-1} (Figure 1).

At this stage, water is capable of deprotonating **4_G** to produce the cyclic phosphodiester intermediate **7_G**. The

dx.doi.org/10.1021/ic300038m | Inorg. Chem. 2012, 51, 8002−8013

Scheme 3

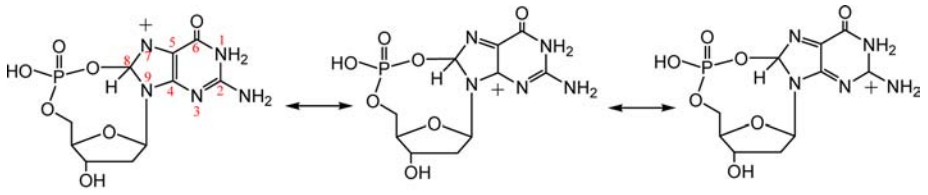

4_G$_a$ 4_G$_b$ 4_G$_c$

energy profile for deprotonation of **4_G** by a three-water cluster is shown in Figure 1b. Our calculations show that the deprotonation process is thermodynamically favorable and requires an overall activation barrier of 81.1 kJ mol^{-1} (Figure 1).

In summary, we propose the mechanism shown in Scheme 2 for the oxidation of 5′-dGMP by Pt^{IV}. In the first step of this reaction, the N7 of guanine binds to Pt^{IV} of [PtCl$_4$(dach)] via substitution of an axial Cl$^-$ ligand by 5′-dGMP. Then, the intramolecular nucleophilic attack of 5′-phosphate to C8 produces intermediate **3_G**. This intermediate cannot be identified experimentally because **3_G** is very unstable and easily undergoes redox reaction through elongation of the Pt−Cl$_{ax}$ bond and generates [Pt^{II}Cl$_2$(dach)], Cl$^-$, and the cationic intermediate **4_G**. Finally, **4_G** is deprotonated by water, and consequently **7_G** is formed.

2. Electron-Transfer Mechanism during the Course of the Guanine Oxidation Starting from 2_G. An analysis of the NBO charge distribution allows us to understand better the mechanism of the redox reaction. In the NBO calculations, the Pt−N7 bond was considered as the *z* axis. As listed in Table 1, there is a significant charge transfer from the guanine moiety to the Pt metal center during the formation of **3_G**. The transferred charge is distributed among the axial Cl ligand and the metal fragment [Pt(Cl$_{eq}$)$_2$(dach)]; 0.147 and 0.137 electrons are transferred to Cl and [Pt(Cl$_{eq}$)$_2$(dach)] on going from **2_G** to **3_G**, respectively. This result suggests that the nucleophilic attack of the phosphate at C8 increases the electron-donating ability of the guanine moiety. The reason for this can be explained by a comparison of the molecular orbitals of the distorted 5′-dGMP moiety in **2_G** and the distorted anionic phosphodiester moiety in **3_G** (Figure 3a,b). Our calculations indicate that the nucleophilic attack of phosphate polarizes almost completely the C8−N7 π bond in the distorted 5′-dGMP toward the N7 atom, increasing the antibonding interaction between N7 and C5 and thereby destabilizing to a large extent the highest occupied molecular orbital (HOMO) in the distorted phosphodiester (from −5.93 eV in the distorted 5′-dGMP to −3.69 eV in the distorted phosphodiester). In such a case, the HOMO level of the distorted phosphodiester lies much higher in energy than the lowest unoccupied molecular orbital (LUMO) level of [PtCl$_3$(dach)]$^+$ (−5.26 eV), causing a large amount of electrons to be transferred through the N7 2p$_z$ orbital to the Pt 5d$_{z^2}$ orbital. Accordingly, our NBO calculation shows that the populations of the N7 2p$_z$ orbital and the guanine moiety decrease while the Pt 5d$_{z^2}$ population increases as one moves from **2_G** to **3_G** (Table 1). The increase of the Pt 5d$_{z^2}$ population in **3_G** results in a more significant repulsive interaction between the d$_{z^2}$ and sp$_z$-hybridized orbital of Cl$_{ax}$ (see HOMO of **3_G** in Figure 3c). The consequence of this increased repulsive interaction is a weakening of the Pt−Cl$_{ax}$ bond and a polarization of the Pt−Cl$_{ax}$ σ bond toward Cl$_{ax}$; the Pt−Cl$_{ax}$ bond is lengthened and the population of 3s and 3p$_z$ valence orbitals increases on going from **2_G** to **3_G**.

We believe that the cyclic phosphodiester moiety in **3_G** is a very strong reducing agent, as evidenced by the considerable destabilization of its HOMO (Figure 3b). Because the very high-lying HOMO is heavily localized on the guanine rings (Figure 3b), the transfer of two electrons from the cyclic phosphodiester to Pt^{IV} causes the guanine to be oxidized. However, it should be noted that, although the phosphodiester moiety in **3_G** is a strong reducing agent, the antibonding interaction between Pt and Cl$_{ax}$ in the HOMO of **3_G** (Figure 3c) reduces the electron-accepting ability of the Pt metal center. The lengthening of the Pt−Cl$_{ax}$ bond in **2TS_G** alleviates the antibonding interaction, thereby enhancing the electron-accepting ability of Pt. In such a case, the Pt−N7 bond is polarized more toward the Pt metal center, leading to an increase in the population of the Pt 5d$_{z^2}$ orbital and a decrease in the population of the N7 2p$_z$ orbital (Table 1). The consequence of this polarization is also reflected in the population changes of subunits in **2TS_G**: Pt(Cl$_{eq}$)$_2$(dach) and Cl$_{ax}$ are populated, while the phosphodiester moiety is depopulated (Table 1).

Once Cl$_{ax}$ has dissociated, two electrons are completely transferred from the guanine moiety of the phosphodiester to Pt^{IV} because of the absence of the antibonding interaction between Cl and Pt, leading to the breaking of the Pt−N7 bond, the oxidation of guanine, and the formation of the cationic intermediate **4_G**. Indeed, Pt^{IV} abstracts the two electrons from the π orbitals of guanine (the HOMO's phosphodiester; Figure 3b), giving the cationic intermediate **4_G**. The H8 deprotonation of **4_G** results in delocalization of the two electrons of the C8−H bond into the oxidized guanine rings in order to compensate for the lack of the two π electrons on the oxidized guanine.

3. Where Does the Stability of the Cationic Intermediate 4_G Arise from? The cationic intermediate **4_G** gains its relative stability from delocalization of the positive charge over the two fused rings, as shown in Scheme 3. In other words, delocalization of the positive charge increases the stability of the cationic intermediate **4_G**, thereby providing a thermodynamic driving force for the guanine moiety to be oxidized. A comparison of the structural parameters of the cyclic phosphodiester fragment in **3_G** and **4_G** provides further evidence for delocalization of the positive charge; the N3−C4 and C5−N7 bonds are shortened, while the C5−C4 and N3−C2 bonds are lengthened. The shortening of the N9−C4 and C2−NH$_2$ bonds in **4_G** can be ascribed to interaction of the lone pairs on the N atoms with the vacant 2p$_\pi$ orbital on the C atoms in the canonical structures **4_G$_b$** and **4_G$_c$**, respectively.

4. Oxidation of 5′-dGMP by [Pt^{IV}Cl$_4$(dach)] via Substitution of an Equatorial Cl Ligand by 5′-dGMP. In

dx.doi.org/10.1021/ic300038m | Inorg. Chem. 2012, 51, 8002−8013

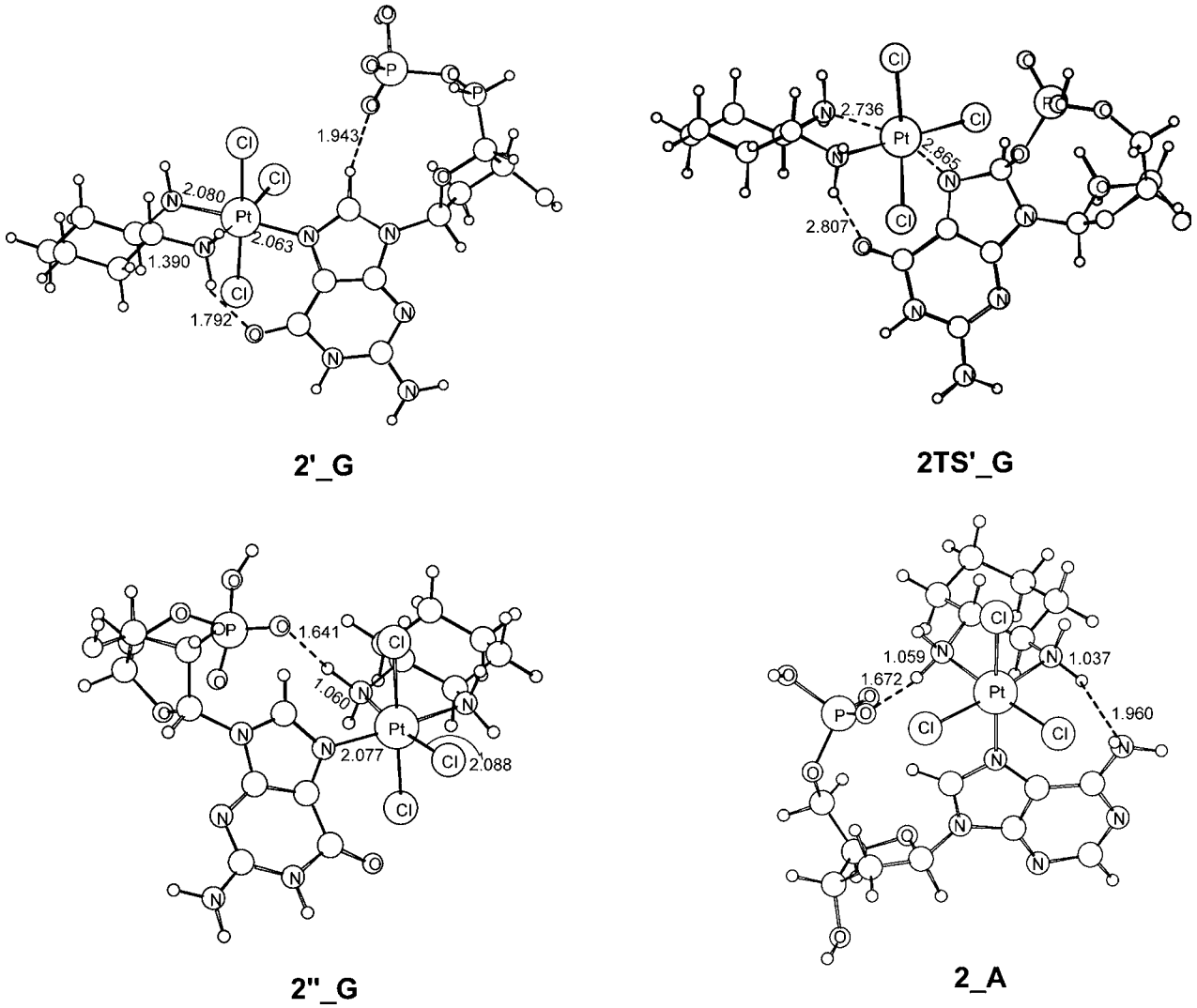

Figure 4. Optimized structures with selected structural parameters (bond lengths in Å) for **2′_G**, **2″_G**, **2′TS_G**, and **2_A**.

the mechanism described above, substitution of one of the axial Cl ligands by 5′-dGMP takes place first and is then followed by the oxidation of guanine. An alternative mechanism involves substitution of one of the equatorial Cl ligands by 5′-dGMP and subsequent redox reaction. Although Choi and co-workers showed that 5′-dGMP is substituted for the axial chloride ligand and not for the equatorial Cl ligand,[17] it is worthwhile to theoretically investigate which of the geometrical isomers undergoes the redox reaction more easily. Substitution of one of the equatorial Cl ligands by 5′-dGMP produces two different stereoisomers (**2′_G** and **2″_G**). These two are distinguished by the type of hydrogen-bonding interaction; in **2′_G**, the hydrogen-bonding interaction exists between the C6O carbonyl and an NH_2 of the dach ligand, while in **2″_G**, the hydrogen-bonding interaction is between phosphate and an NH_2 of the dach ligand (Figure 4). It is interesting to note that, although the Pt−N7 bond in **2_G** is longer than that in both the stereoisomers **2′_G** and **2″_G** (Figures 2 and 4), **2_G** is calculated to be more stable than **2′_G** and **2″_G**. The higher stability of **2_G** is likely related to the coexistence of the NH−C6O and NH−phosphate hydrogen-bonding interactions in **2_G**. The energy profiles for the redox reactions from adducts **2′_G** and **2″_G** are shown in Figures 5 and S1 in the Supporting Information, respectively.

Figure 5 shows that the intermediate **3′_G** is formed via the nucleophilic attack of phosphate at C8, which occurs through transition structure **1′TS_G** with an overall barrier of 130.9 kJ mol^{-1}. The reaction Gibbs energy for the conversion of **2′_G** to **3′_G** (107.3 kJ mol^{-1}; Figure 5) is almost the same as that for the conversion of **2_G** to **3_G** (103.2 kJ mol^{-1}; Figure 1). This is understandable because the reaction energy is primarily controlled by the energy required for disruption of the π-electron delocalization in the five-membered ring of the guanine. The redox reaction starting from **3′_G** takes place via transition structure **2′TS_G** with a barrier of 48.7 kJ mol^{-1}. This barrier is calculated to be 21.0 kJ mol^{-1} larger than the analogous barrier from **3_G**. Our calculations show that the guanine oxidation process through **2′_G** is kinetically less favorable than that through **2_G**; the rate of the redox reaction at 298 K from **2′_G** is predicted to be nearly 3.3×10^7 times less than that from **2_G**.

After crossing transition structure **2′TS_G**, the redox reaction is completed and the platinum(II) square-planar species **9** is formed as the initial product. Because two electrons are transferred along the Pt−N7 axis during the course of the redox reaction, one of the arms of the dach ligand rather than a Cl^- ligand is detached in the initial product **9**. This species is not stable and can convert to **8** through the attack of the

dx.doi.org/10.1021/ic300038m | Inorg. Chem. 2012, 51, 8002−8013

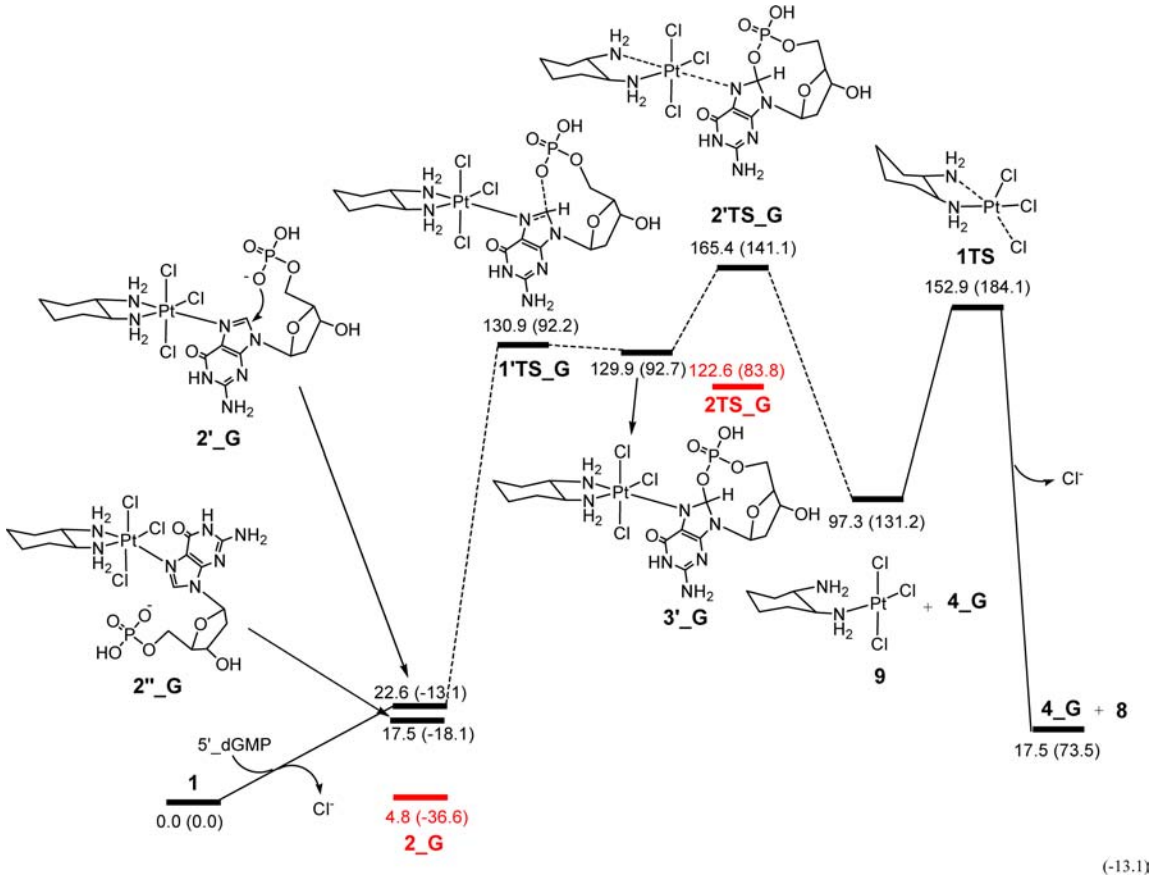

Figure 5. Energy profile calculated for the oxidation of 5′-dGMP by Pt^{IV} starting from the stereoisomer **2′_G**. The relative free energies and electronic energies (in parentheses) obtained from the B3LYP/BS2//B3LYP/BS1 calculations are given in kJ mol^{-1}.

pendant NH_2 of dach at the platinum of **9** with a concomitant release of Cl; **9** is computed to be 79.8 kJ mol^{-1} less stable than **8** + Cl^- at the B3LYP level of theory.

On the basis of these results, one may conclude that the activation barrier of the redox step is mainly affected by the energy of the relevant initial products; the less stable the initial product, the higher the activation barrier. That is, **3′_G** undergoes the redox reaction with more difficulty than **3_G** because **9** is less stable than **8** (see Figures 1 and 5). The lesser stability of **9** also renders **2′TS_G**, a later transition structure than **2TS_G**; the Pt−N7 bond in **2′TS_G** is 0.351 Å longer than that in **2TS_G** (Figures 2 and 4).

The more difficult redox reaction from **3′_G** can also be attributed to the weaker acidic character of the Pt metal center in this intermediate; the LUMO of the distorted $[PtCl_3(dach)]^+$ moiety in **3′_G** lies much higher in energy than that in **3_G**, indicating that the antibonding interaction between N and Pt in the LUMO of the distorted $[PtCl_3(dach)]^+$ moiety in **3′_G** is more significant than that between Cl and Pt in the LUMO of the distorted $[PtCl_3(dach)]^+$ moiety in **3_G** (Figure 6a,b). In order for the Pt^{IV} metal center in **3′_G** to be reduced to Pt^{II}, a larger deformation of the metal fragment $PtCl_3(dach)$ in the transition structure (primarily the lengthening of the Pt−N bond) is necessarily required; the Pt−N bond is elongated by 0.563 Å on going from **3′_G** to **2′TS_G**, while the Pt−Cl bond is elongated by 0.466 Å on going from **3_G** to **2TS_G**. The larger deformation causes the energy of the LUMO of the distorted $[PtCl_3(dach)]^+$ moiety in **2′TS_G** to be almost the same as that in **2TS_G** (Figure 6c,d). The larger the deformation of the $PtCl_3(dach)$ moiety, the later the transition structure and the higher the activation barrier of the redox step.

The brief summary of this section is that the Pt^{IV}−G adduct derived from replacement of the equatorial Cl ligand of $[Pt^{IV}Cl_4(dach)]$ with 5′-dGMP is less reactive toward the redox reaction than that of the adduct derived from replacement of the axial Cl ligand.

5. Oxidation of 5′-dAMP by $[Pt^{IV}Cl_4(dach)]$. As stated in the Introduction, only guanine nucleotides have been reported so far to be reactive toward oxidation. To see whether the adenine nucleotides are susceptible to oxidation, we replaced 5′-dGMP with 5′-dAMP and investigated the effect of the replacement on the potential energy surface of the redox reaction (Figure 7). The oxidation of 5′-dAMP by Pt^{IV} has a higher activation energy by 59.0 kJ mol^{-1} than that of 5′-dGMP, suggesting that the oxidation of 5′-dAMP is kinetically less favorable.

Our calculations show that 5′-dAMP coordinates to Pt^{IV} more weakly than 5′-dGMP, a result that can be attributed to the lower electron-donating ability of adenine as well as the weaker hydrogen-bonding interaction[22] in **2_A**. The lower electron-donating ability of adenine in **2_A** is reflected in a longer Pt−N7 bond distance (2.090 Å; Figure 4) and a more negative NBO charge on 5′-dAMP (−0.461); in **2_G**, the Pt−N7 bond distance and NBO charge on 5′-dGMP are 2.088 Å and −0.424, respectively. The NH_2−C6X hydrogen-bonding interaction in **2_A** (X = NH_2) is weaker than that in **2_G** (X =

dx.doi.org/10.1021/ic300038m | Inorg. Chem. 2012, 51, 8002−8013

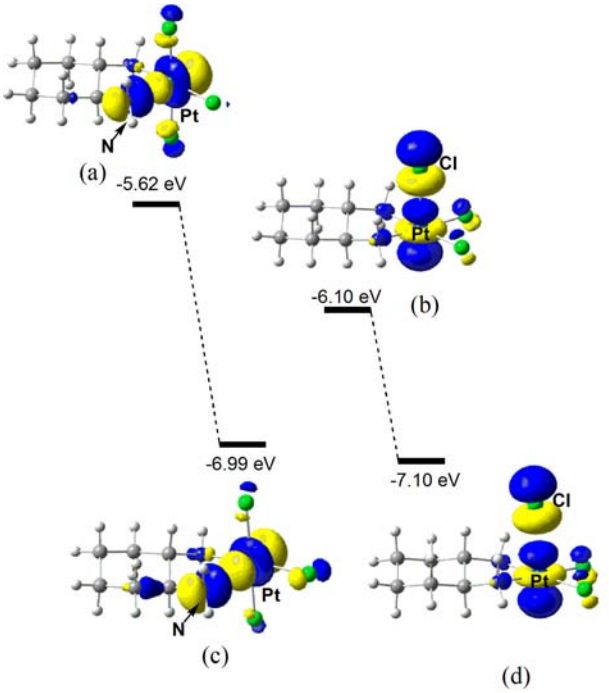

Figure 6. Spatial plots and energies of the LUMO of the distorted $[PtCl_3(dach)]^+$ moiety in (a) **3′_G**, (b) **3_G**, (c) **2′TS_G**, and (d) **2TS_G**. Elongation of the Pt−N distance in **2′TS_G** and the Pt−Cl distance in **2TS_G** causes the LUMO of the distorted $[PtCl_3(dach)]^+$ moiety to fall in energy, resulting in the increased electron-accepting ability of the Pt metal center from the anionic phosphodiester.

O); the H···NC6 distance in **2_A** (1.960 Å; Figure 4) is much longer than the H···OC6 distance in **2_G** (1.715 Å; Figure 2).

Starting from **2_A**, the reaction energy for the nucleophilic attack of phosphate at the C8 atom of the adenine complex is calculated to be 108.9 kJ mol^{-1}, an energy value that is fairly close to that of the guanine complex (103.3 kJ mol^{-1}; Figures 1 and 7).[18] This similarity suggests that the energy required for disruption of the π-electron delocalization in the five-membered ring of both nucleobases is almost the same. However, the redox step for adenine is about 16.5 kJ mol^{-1} less favorable than that for guanine. The conversion of **3_A** → **4_A** + $Pt(dach)Cl_2$ + Cl^- (77.7 kJ mol^{-1}; Figure 7) is also less exergonic than that of **3_G** → **4_G** + $Pt(dach)Cl_2$ + Cl^- (90.6 kJ mol^{-1}; Figure 1). A similar behavior is obtained when the M06 calculation is used (Figures S2 and S5 in the Supporting Information). This finding is consistent with the argument above that there is a correlation between the activation barrier of the redox step and the energy of the initial redox product. It follows from these results that the adenine nucleotide is less susceptible to oxidation compared to the guanine nucleotide, although the overall redox reaction (formation of the neutral phosphodiesters **7_A** and **7_G**) for both nucleotides is thermodynamically feasible (see Figures 1 and 7).

The lesser reactivity of the adenine nucleotide toward oxidation can be attributed to the disruption of the aromatic π system of the six-membered ring[23,24] of the phosphodiester in **2TS_A** and **4_A**, which is a destabilizing factor. The cyclic phosphodiester moiety in transition structure **2TS_A** carries a positive NBO charge of 0.289 and consequently becomes partly cationic in character. Therefore, delocalization of the partial positive charge over the two fused rings in **2TS_A** helps to increase the stability of the system (Scheme 4). However, as is evident from Scheme 4, delocalization disrupts the aromaticity of the six-membered ring of the phosphodiester moiety in the transition structure **2TS_A**, as supported by the small NICS values for the ring [NICS(0) +0.4, NICS(1) −3.5, and $NICS_{zz}(1)$ −6.1 ppm]. The NICS(0), NICS(1), and $NICS_{zz}(1)$ values for the six-membered ring of 5′-dAMP in **2_A** are computed to be −7.8, −9.2, and −23.8 ppm, respectively, indicating that the ring is aromatic at the beginning of the reaction. In contrast, the aromaticity of the six-membered ring of 5′-dGMP in **2_G** is negligible [NICS(0) −3.8, NICS(1) −3.7 and $NICS_{zz}(1)$ −6.5 ppm]; thus, delocalization of the partial positive charge in **2TS_G** (Figure 1) is not destabilizing.

From these results, we can conclude that 5′-dAMP is much less reactive toward oxidation than 5′-dGMP because, first, 5′-dAMP is coordinated to Pt^{IV} much more weakly than 5′-dGMP and, second, the two-electron-transfer process to Pt^{IV} in the 5′-dAMP system results in a decrease of the aromaticity of the six-membered ring of the cationic phosphodiester moiety, making the redox step much more difficult.

6. Hydrolysis of the Cyclic Phosphodiester Intermediate to 8-oxo-dGMP. As mentioned in the Introduction, the cyclic phosphodiester intermediate **7_G** is not stable and hydrolyzes to 8-oxo-dGMP. Choi and co-workers showed that the hydrolysis process is greatly accelerated in acidic media. We have calculated various possibilities for the hydrolysis process, and we find that in order for hydrolysis to occur, N7 of **7_G** should be protonated first. The protonation of N7 polarizes the N7−C8 π bond toward N7 and causes a lone pair of O1 to interact with the $2p_\pi$ orbital of C8; from **7_G** to **11_G**, the N7−C8 bond is elongated while the C8−O1 bond is shortened (Figure 8). This interaction, which results in a weakening of the P−O1 bond, allows the hydrolysis reaction to occur easily.

Our calculations show that the protonation of **7_G** by H_3O^+ in order to produce **11_G** is a facile process (Figure 9). This reaction is calculated to be exergonic and occurs without barrier. The hydrolysis is completed via the barrierless attack of water on the P atom of **12_G** in an S_N2 fashion. These results predict that the hydrolysis reaction should be very fast in an acidic media, a result that is consistent with the experiment.[18] As expected, the water molecule is not sufficiently acidic to protonate the N7 atom.[25] Therefore, the hydrolysis reaction at pH 7 is very slow.

■ CONCLUSION

DFT calculations have been carried out to investigate the mechanism of oxidation of 5′-dGMP and 5′-dAMP by $[Pt^{IV}Cl_4(dach)]$. This study has identified several important conclusions as follows:

(1) The overall reaction mechanism of the oxidation of 5′-dGMP by Pt^{IV} proceeds as follows. In the first step, the N7 of guanine binds to Pt^{IV} of $[PtCl_4(dach)]$ via substitution of an axial Cl^- ligand by 5′-dGMP. Next, the intramolecular nucleophilic attack of 5′-phosphate to C8 produces intermediate **3_G**. This intermediate cannot be deprotonated by water and instead undergoes a redox reaction through elongation of the Pt−Cl_{ax} bond, which generates $[Pt^{II}Cl_2(dach)]$, Cl^-, and the cationic phosphodiester intermediate **4_G**. Finally, **4_G** is deprotonated by water, and the cyclic phosphodiester **7_G** is formed, which is then hydrolyzed to the final oxidized product.

dx.doi.org/10.1021/ic300038m | Inorg. Chem. 2012, 51, 8002−8013

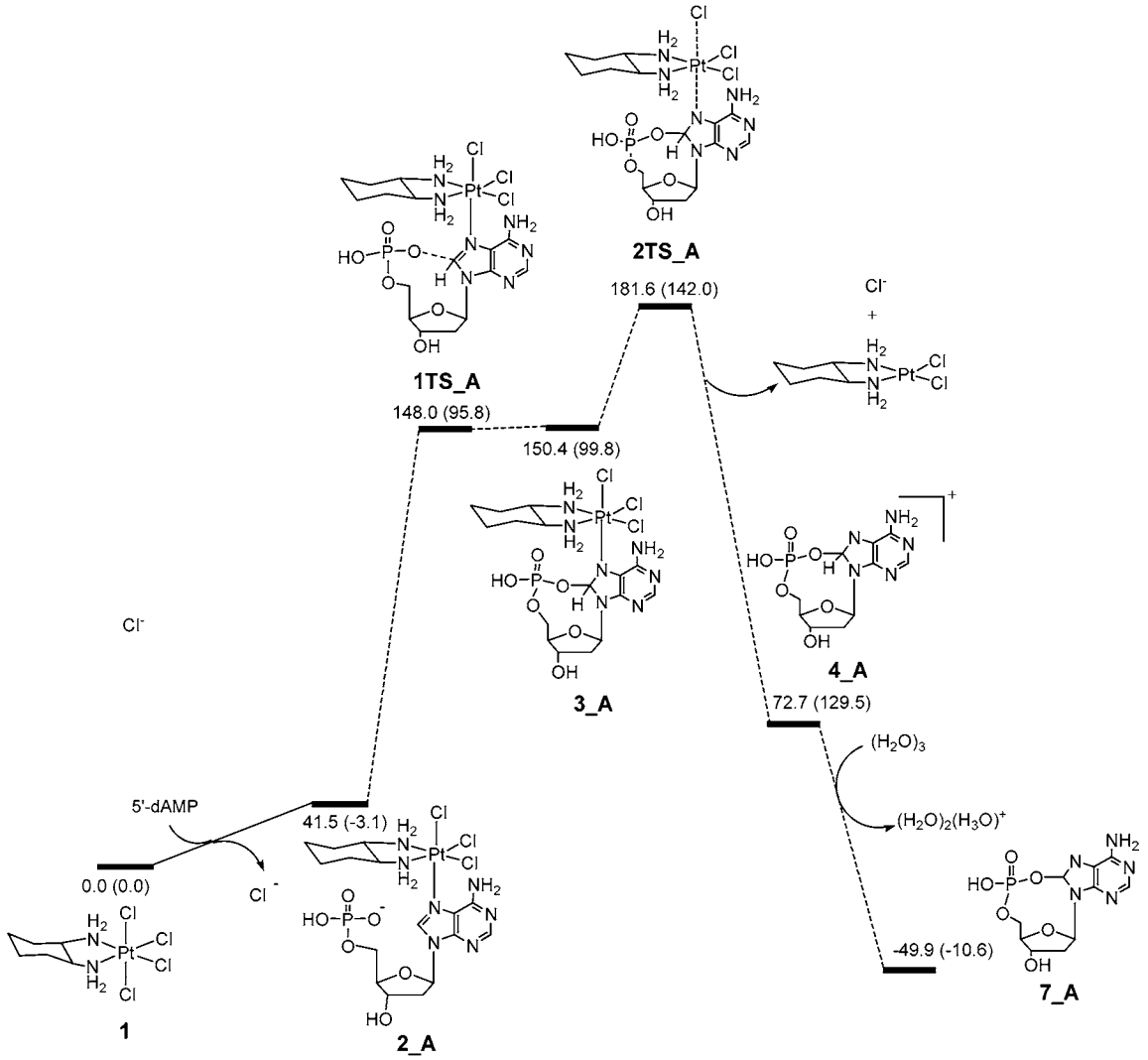

Figure 7. Energy profile calculated for the oxidation of 5′-dAMP by $[Pt^{IV}Cl_4(dach)]$, leading to the formation of **6_A**. The relative free energies and electronic energies (in parentheses) obtained from the B3LYP/BS2//B3LYP/BS1 calculations are given in kJ mol^{-1}.

Scheme 4

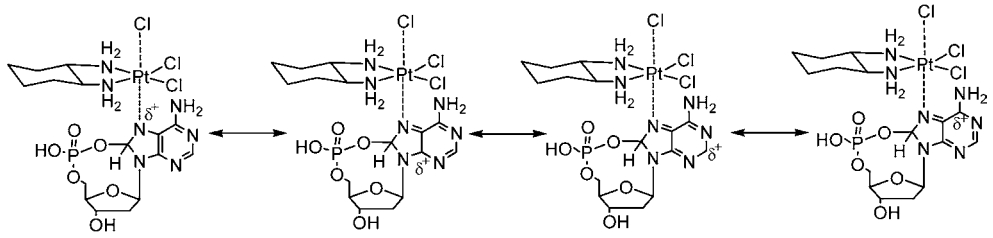

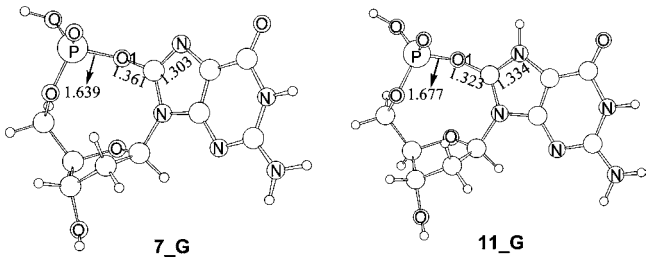

Figure 8. Optimized structures with selected structural parameters (bond lengths in Å) for **7_G** and **11_G**.

(2) The two intermediates **3_G** and **4_G**, which are unknown experimentally, are predicted to be formed during the guanine oxidation reaction. We believe that the experimental identification of these two intermediates is very difficult because their lifetimes are not long enough; the energies of **3_G** and **4_G** are calculated at both the B3LYP and M06 levels of theory to lie significantly higher than that of **2_G**.

(3) Intermediate **4_G** is responsible for the formation of the phosphodiester, rather than **3_G** as suggested in the literature.

dx.doi.org/10.1021/ic300038m | *Inorg. Chem.* 2012, 51, 8002−8013

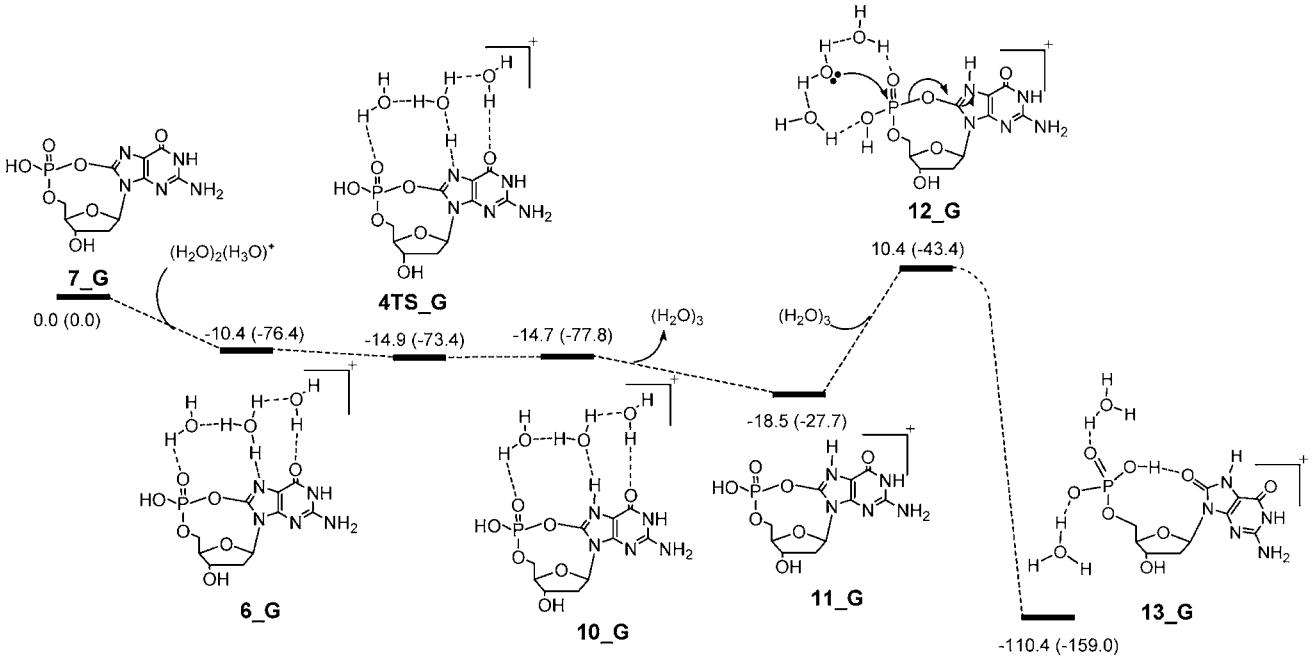

Figure 9. Energy profile calculated for the hydrolysis of the cyclic phosphodiester to 8-oxo-dGMP in the presence of H_3O^+. The relative free energies and electronic energies (in parentheses) obtained from the B3LYP/BS2//B3LYP/BS1 calculations are given in kJ mol^{-1}.

(4) The electron transfer from guanine to Pt^{IV} is driven by dissociation of the axial Cl^- ligand in **3_G**.
(5) The Pt^{IV}–G adduct derived from replacement of the equatorial Cl ligand of $[Pt^{IV}Cl_4(dach)]$ with 5′-dGMP is much less reactive toward the redox reaction than the adduct derived from replacement of the axial Cl ligand. This is mainly because of the weaker acidic character of the Pt metal center in **3′_G** than in **3_G**.
(6) The Pt^{IV}-coordinated 5′-dAMP is much less reactive toward oxidation than the Pt^{IV}-coordinated 5′-dGMP because, first, 5′-dAMP is coordinated to Pt^{IV} much more weakly than 5′-dGMP and, second, the two-electron-transfer process in the 5′-dAMP system results in a decrease of the aromaticity of the six-membered ring of the cationic phosphodiester moiety, thus making the redox step much more difficult.
(7) The only feasible pathway for hydrolysis of the cyclic phosphodiester intermediate to 8-oxo-dGMP is via the initial protonation of N7. The protonation by H_3O^+ is an exothermic process, while that by water is greatly endothermic.

■ ASSOCIATED CONTENT

Supporting Information

Text giving the complete ref 5, Figures S1–S10, the arguments related to the oxidation of 5′-dGMP from **2″_G**, exploring an alternative mechanism for the oxidation of 5′-dGMP, and tables giving Cartesian coordinates of all optimized structures along with energies and imaginary frequencies. This material is available free of charge via the Internet at http://pubs.acs.org.

■ AUTHOR INFORMATION

Corresponding Author

*E-mail: ariafard@yahoo.com (A.A.), Brian.Yates@utas.edu.au (B.F.Y.).

Notes

The authors declare no competing financial interest.

■ ACKNOWLEDGMENTS

We thank the Australian Research Council for financial support and the Australian National Computational Infrastructure and University of Tasmania for computing resources. A.A., S.A., E.S.T., and S.N. are grateful for financial support of the Islamic Azad University, Central Tehran Branch.

■ REFERENCES

(1) (a) Cadet, J.; Douki, T.; Ravanat, J.-L. *Acc. Chem. Res.* **2008**, *41*, 1075. (b) Kanvah, S.; Joseph, J.; Schuster, G. B.; Barnett, R. N.; Cleveland, C. L.; Landman, U. *Acc. Chem. Res.* **2010**, *43*, 280.
(2) (a) Kawanishi, S.; Hiraku, Y.; Oikawa, S. *Mutat. Res., Rev. Mutat. Res.* **2001**, *488*, 65. (b) Wallace, S. S. *Free Radical Biol. Med.* **2002**, *33*, 1. (c) Franco, R.; Schoneveld, O.; Georgakilas, A. G.; Panayiotidis, M. I. *Cancer Lett.* **2008**, *266*, 6.
(3) (a) Roat, R. M.; Reedijk, J. *J. Inorg. Biochem.* **1993**, *52*, 263. (b) Muller, J. G.; Zheng, P.; Rokita, S. E.; Burrows, C. J. *J. Am. Chem. Soc.* **1996**, *118*, 2320. (c) Rodriguez-Bailey, V. M.; LaChance-Galang, K. J.; Doan, P. E.; Clarke, M. J. *Inorg. Chem.* **1997**, *36*, 1873. (d) Burrows, C. J.; Muller, J. G. *Chem. Rev.* **1998**, *98*, 1109. (e) Farrer, B. T.; Thorp, H. H. *Inorg. Chem.* **2000**, *39*, 44. (f) Farrer, B. T.; Thorp, H. H. *Inorg. Chem.* **2000**, *39*, 44. (g) Li, L.; Karlin, K. D.; Rokita, S. E. *J. Am. Chem. Soc.* **2005**, *127*, 520. (h) Pratviel, G.; Meunier, B. *Chem.—Eur. J.* **2006**, *12*, 6018. (i) Olmon, E. D.; Sontz, P. A.; Blanco-Rodríguez, A. M.; Towrie, M.; Clark, I. P.; Vlček, A., Jr.; Barton, J. K. *J. Am. Chem. Soc.* **2011**, *133*, 13718. (j) Choi, S.; Ryu, D. W.; DellaRocca, J. G.; Wolf, M. W.; Bogart, J. A. *Inorg. Chem.* **2011**, *50*, 6567.
(4) (a) Choi, S.; Filotto, C.; Bisanzo, M.; Delaney, S.; Lagasee, D.; Whitworth, J. L.; Jusko, A.; Li, C.; Wood, N. A.; Willingham, J.; Schwenker, A.; Spaulding, K. *Inorg. Chem.* **1998**, *37*, 2500. (b) Choi, S.; Mahalingaiah, S.; Delaney, S.; Neale, N. R.; Masood, S. *Inorg. Chem.* **1999**, *38*, 1800. (c) Choi, S.; Cooley, R. B.; Hakemian, A. S.; Larrabee, Y. C.; Bunt, R. C.; Maupaus, S. D.; Muller, J. G.; Burrows, C. J. *J. Am. Chem. Soc.* **2004**, *126*, 591. (d) Choi, S.; Cooley, R. B.; Voutchkova, A.; Leung, C. H.; Vastag, L.; Knowles, D. E. *J. Am. Chem. Soc.* **2005**, *127*,

1773. (e) Choi, S.; Vastag, L.; Leung, C. H.; Beard, A. M.; Knowles, D. E.; Larrabee, J. A. *Inorg. Chem.* **2006**, *45*, 10108. (f) Choi, S.; Personick, M. L.; Bogart, J. A.; Ryu, D. W.; Redman, R. M.; Laryea-Walker, E. *Dalton Trans.* **2011**, *40*, 2888.

(5) Frisch, M. J.; et al. *Gaussian 09*, revision A.02; Gaussian, Inc.: Wallingford, CT, 2009.

(6) Barone, V.; Cossi, M. *J. Phys. Chem. A* **1998**, *102*, 1995.

(7) (a) Lee, C. T.; Yang, W. T.; Parr, R. G. *Phys. Rev. B* **1988**, *37*, 785. (b) Miehlich, B.; Savin, A.; Stoll, H.; Preuss, H. *Chem. Phys. Lett.* **1989**, *157*, 200. (c) Becke, A. D. *J. Chem. Phys.* **1993**, *98*, 5648.

(8) (a) Hay, P. J.; Wadt, W. R. *J. Chem. Phys.* **1985**, *82*, 270. (b) Wadt, W. R.; Hay, P. J. *J. Chem. Phys.* **1985**, *82*, 284.

(9) Hariharan, P. C.; Pople, J. A. *Theor. Chim. Acta* **1973**, *28*, 213.

(10) Ehlers, A. W.; Böhme, M.; Dapprich, S.; Gobbi, A.; Höllwarth, A.; Jonas, V.; Köhler, K. F.; Stegmann, R.; Veldkamp, A.; Frenking, G. *Chem. Phys. Lett.* **1993**, *208*, 111.

(11) (a) Fukui, K. *J. Phys. Chem.* **1970**, *74*, 4161. (b) Fukui, K. *Acc. Chem. Res.* **1981**, *14*, 363.

(12) (a) Zhao, Y.; Schultz, N. E.; Truhlar, D. G. *J. Chem. Theory Comput.* **2006**, *2*, 364. (b) Zhao, Y.; Truhlar, D. G. *J. Chem. Phys.* **2006**, *125*, 194101. (c) Zhao, Y.; Truhlar, D. G. *J. Phys. Chem. A* **2006**, *110*, 13126.

(13) Weigend, F.; Furche, F.; Ahlrichs, R. *J. Chem. Phys.* **2003**, *119*, 12753.

(14) Glendening, E. D.; Read, A. E.; Carpenter, J. E.; Weinhold, F. *NBO*, version 3.1; Gaussian, Inc.: Pittsburgh, PA, 2003.

(15) Berners-Price, S. J.; Frey, U.; Ranford, J. D.; Sader, P. J. *J. Am. Chem. Soc.* **1993**, *115*, 8649.

(16) Wei, C. S.; Jiménez-Hoyos, C. A.; Videa, M. F.; Hartwig, J. F.; Hall, M. B. *J. Am. Chem. Soc.* **2010**, *132*, 3078.

(17) Choi, S.; Vastag, L.; Larrabee, Y. C.; Personick, M. L.; Schaberg, K. B.; Fowler, B. J.; Sandwick, R. K.; Rawji, G. *Inorg. Chem.* **2008**, *47*, 1352.

(18) In Figures 1, 7, and 9, the transition structures **1TS_G**, **1TS_A**, and **4TS_G** are located below their corresponding reactant(s). This arises from the procedure for doing the single-point calculations. At the geometry optimization level of theory, the transition structure is indeed higher in energy than the reactants, as it should be. However, when the entropy effects are taken into consideration and single-point calculations are carried out with a much larger basis set (a procedure that is needed to give robust results), the transition structure ends up slightly lower than the reactant(s). What this indicates in practice is that the transition structure and the reactants are probably very close in energy, and at some levels of theory, the transition structure will not exist.

(19) The pathway involving the nucleophilic attack of the O1 atom of 5′-phosphate to the C8 atom is found to be unlikely. In this pathway, the hydrogen-bonding interaction between O1 and the NH_2 of dach is disrupted. The transition structure located for this pathway lies ∼ 26 kJ mol^{-1} higher in energy than the transition structure **1TS_G**.

(20) Shi, F.-Q.; Li, X.; Xia, Y.; Zhang, L.; Yu, Z.-X. *J. Am. Chem. Soc.* **2007**, *129*, 15503.

(21) In the case when oxidation of the guanine is initiated by OH^-, the kinetic isotope effect of 7.2 has been obtained experimentally by Choi et al (see ref 4f). This indicates that the H8 deprotonation should be involved in the rate-determining step, which is different from the findings in this work. This difference is most likely due to the strong basicity of OH^- in the work by Choi. In the presence of OH^-, we predict that the H8 deprotonation of the Pt^{IV}-bound guanine will occur upon the nucleophilic attack of the base at C8. However, according to our calculations, this alternative mechanism for oxidation of 5′-dGMP lies higher in energy at the levels of theory that we have used (Figures S7−S10 in the Supporting Information).

(22) Burda et al. investigated the interactions between Pt^{II} and purine DNA bases and suggested that the smaller dipole moment of adenine and its unfavorable orientation are the reasons why the platinum(II) adenine adducts are less stable than the platinum(II) guanine adducts. (a) Pavelka, M.; Burda, J. V. *J. Mol. Model.* **2007**, *13*, 367. (b) Burda, J. V.; Leszczynski, J. *Inorg. Chem.* **2003**, *42*, 7162.

(23) Previous theoretical studies showed that the six-membered ring of adenine is aromatic. For example, see: Huertas, O.; Poater, J.; Fuentes-Cabrera, M.; Orozco, M.; Sola, M.; Luque, F. J. *J. Phys. Chem. A* **2006**, *110*, 12249.

(24) Our calculations showed that the energy required for the removal of two electrons from adenine (13.61/13.71 eV) is higher than that from guanine (12.90/13.01 eV). The higher energy required for oxidation of adenine can be ascribed to disruption of the aromaticity of the six-membered ring of adenine; NICS values for the six-membered ring of $adenine^{2+}$ are computed as NICS(0) +8.7, NICS(1) +1.9, and $NICS_{zz}(1)$ +11.0 ppm.

(25) The reaction of **7_G** + $(H_2O)_3$ → **11_G** + $(H_2O)_2(OH^-)$ is calculated to be very endergonic (ΔG = 131.8 kJ mol^{-1}).